Journal of The Electrochemical Society, **158** (2) D49-D53 (2011)
0013-4651/2010/158(2)/D49/5/$28.00 © The Electrochemical Society

Cu/Multiwalled Carbon Nanotube Composite Films Fabricated by Pulse-Reverse Electrodeposition

Susumu Arai,[a,*,z] Yoriyuki Suwa,[a] and Morinobu Endo[b]

[a]*Department of Chemistry and Material Engineering and* [b]*Department of Electrical and Electronic Engineering, Faculty of Engineering, Shinshu University, Nagano 380-8553, Japan*

Cu/multiwalled carbon nanotube (MWCNT) composite plating by a pulse-reverse (PR) electrodeposition method was investigated in order to increase the MWCNT content of the composite plating films. The electrodeposition and dissolution behaviors of the composite films were investigated using scanning electron microscopy and X-ray diffraction to determine the most suitable electrodeposition and dissolution current densities for PR electrodeposition. PR electrodeposition of the Cu/MWCNT composite films was conducted by varying the current reverse ratios at the most suitable electrodeposition and dissolution current densities. The surface morphology of the Cu/MWCNT composite films after dissolution was significantly changed by variation of the anodic current densities. The MWCNT content of the composite films formed by PR electrodeposition was greater than that obtained using a direct current (dc) electrodeposition method, and reached a maximum value of 0.59 mass %, which is a 40% increase over that for dc electrodeposition. Furthermore, the surface roughness of the composite films fabricated by PR electrodeposition was less than that by dc electrodeposition.
© 2010 The Electrochemical Society. [DOI: 10.1149/1.3518414] All rights reserved.

Manuscript submitted July 8, 2010; revised manuscript received October 25, 2010. Published December 2, 2010.

Cu plating has been widely used in the electronics industry, mainly due to its superior electrical and thermal conductivity. In particular, the development of "via-filling" for printed-circuit boards and "superfilling" for the damascene process by Cu electrodeposition have been vigorously advanced.[1-14]

Carbon nanotubes[15,16] (CNTs) have excellent mechanical characteristics, such as high tensile strength and elastic modulus, and also exhibit high thermal and electrical conductivity values. Research into practical applications of CNTs, such as the preparation of resin/CNT, ceramic/CNT, and metal/CNT composites, has therefore been actively pursued. Recently, fabrication of metal/CNT composites has been attempted using plating techniques.[17-25]

The present authors and others have reported that Cu/multiwalled CNT (MWCNT) composites can be electrodeposited, and the deposits tend to have bumpy[26-28] or powdery[29] morphology, due to the intrinsic and unique electronic conduction of the CNTs.[30] CNTs have higher thermal conductivity than Cu; therefore, Cu/CNT composite films are expected to exhibit higher thermal conductivity than pure Cu films. However, Cu itself has high thermal conductivity; therefore, it is not expected that a Cu/CNT composite film containing a small amount of CNTs would exhibit obviously higher thermal conductivity than a pure Cu plating film.[28] Therefore, an increase of the CNT content in Cu/CNT composite plating films is very important to increase the thermal conductivity of Cu/CNT composite plating films over that of pure Cu films.

In general, the pulse-reverse (PR) electrodeposition method is used to smooth the surface morphology of plating films. If the PR electrodeposition method is applied to composite plating with granular or spherically shaped nanoparticles, then most nanoparticles could be separated from the composite film during dissolution of the metal matrix. Therefore, an increase of the particle content in a composite film cannot be expected for composite films employing granular or spherically shaped nanoparticles with PR electrodeposition. However, CNTs have a fibrous shape; therefore, it would be expected that the CNTs would not be separated from the composite film, due to entanglement with each other during the metal matrix dissolution process. Therefore, PR electrodeposition of a metal/CNT composite plating film could increase the CNT content of the composite film over conventional methods. The fabrication of Ni/CNT composite plating films has been reported.[31,32] However, the fabrication of Cu/CNT composite films using PR electrodeposition has not been reported.

In this study, the PR electrodeposition of Cu/MWCNT composite films was examined with a main focus on increasing the MWCNT content of the composite films.

Experimental

The CNTs used in the present study were commercially available vapor-grown MWCNTs (Showa Denko Co., Ltd., Japan), formed via catalyst-assisted chemical vapor deposition[33] (CVD) and heat-treated at 2800°C in Ar atmosphere for 30 min. The MWCNTs were typically 150 nm in diameter and 15 μm in length. A sulfuric Cu plating bath (0.85 mol dm^{-3} $CuSO_4 \cdot 5H_2O$ + 0.55 mol dm^{-3} H_2SO_4) was used as the base bath. The MWCNTs did not disperse uniformly in the base bath; however, a homogeneous dispersion of MWCNTs was achieved by the addition of a dispersant [poly(acrylic acid), mean molecular weight 5000, PA5000)][25-29] to the base bath with stirring. The composition of the Cu/MWCNT composite plating bath was 0.85 mol dm^{-3} $CuSO_4 \cdot 5H_2O$ + 0.55 mol dm^{-3} H_2SO_4 + 100ppm PA5000 + 2 g dm^{-3} MWCNTs. A commercially available electrolytic cell (Microcell model I, Yamamoto-Ms Co., Ltd., Japan), with internal dimensions of 65 × 65 × 95 mm was employed for the electrodeposition. The volume of the plating bath was 250 cm^3. A pure Cu plate with an exposed surface area of 10 cm^2 (3 × 3.33 cm^2) was mainly used as the substrate. A Cu plate containing a small amount of phosphorus was used as the anode. Electrodeposition behavior was examined under galvanostatic conditions in the range of cathodic current density from 0.5 to 5 A dm^{-2} with agitation by bubbling air. Agitation was effective to suppress the sedimentation of MWCNTs; that is, to disperse MWCNTs homogeneously in the plating bath. The microcell model I has holes at the bottom for agitation by air bubbling, and air bubbling was conducted using an exclusive air pump (Hull cell air pump, Yamamoto-Ms Co., Ltd., Japan). The dissolution behavior of the electrodeposited Cu/MWCNT composite films was examined under galvanostatic conditions in the range of anodic current density from 1 to 20 A dm^{-2} with agitation by bubbling air. PR electrodeposition was performed using an electrochemical measurement system (HZ-5000, Hokuto Denko Corp., Japan) with agitation by bubbling air. The bath temperature for all experiments was 25°C.

The microstructure of the Cu/MWCNT composite films was examined using a field-emission scanning electron microscope (FE-SEM, JEOL JSM-7000F). A cross-section polisher (JEOL SM-09010) was used to prepare cross-sectional samples for observations. The phase structures of the films were examined using X-ray diffraction (XRD) with Cu $K\alpha_1$ radiation (XRD-6000, Shimadzu Corp., Japan).

The MWCNT content in the composite films was determined by direct weighing. For the weight measurement, thick Cu/MWCNT

* Electrochemical Society Active Member.
z E-mail: araisun@shinshu-u.ac.jp

Downloaded 02 Dec 2010 to 160.252.86.17. Redistribution subject to ECS license or copyright; see http://www.ecsdl.org/terms_use.jsp

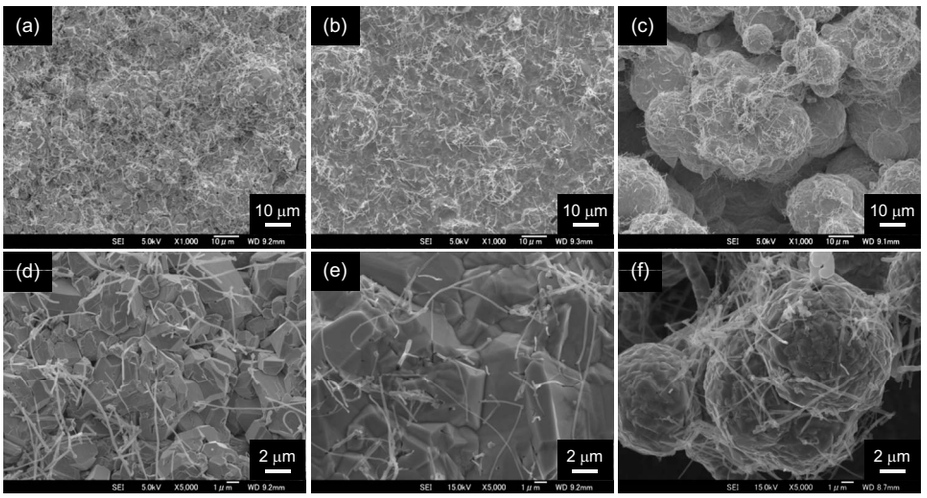

Figure 1. Surface FE-SEM images of Cu/MWCNT composite films electrodeposited at various current densities of (a) 0.5, (b) 1, and (c) 5 A dm^{-2}. The images in (d)–(f) are high magnification images of (a)–(c), respectively. The quantity of cathodic electricity used was 600 C.

composite films (over 2 g) were electrodeposited on stainless steel substrates. After separation from the substrates, the Cu matrix of the films was dissolved in nitric acid. The MWCNTs in the nitric acid solution were then filtered, dried, and weighed.

Results and Discussion

Figure 1 shows surface FE-SEM images of composite films electrodeposited at various current densities from the Cu/MWCNT composite plating bath. The quantity of electricity was 600 C, which corresponds to a film thickness of approximately 20 μm. Relatively flat surface morphology was observed for deposition at 0.5 A dm^{-2} and particularly at 1 A dm^{-2}, whereas bumpy and spherical morphology was observed for deposition at 5 A dm^{-2}.[30] Therefore, the electrodeposition current density for PR electrodeposition was fixed at 1 A dm^{-2} for further experiments. FE-SEM observation revealed that the amount of MWCNTs on the composite film surfaces electrodeposited at 1 A dm^{-2} did not change significantly beyond an electricity quantity of 300 C, which corresponds to a film thickness of around 10 μm.

Figure 2 shows surface FE-SEM images of Cu/MWCNT composite films after electrochemical dissolution of the composite films, i.e., the Cu matrix, at various anodic current densities. The Cu/MWCNT composite film was fabricated at 1 A dm^{-2} before dissolution and the thickness was around 20 μm (Fig. 2a). The quantity of anodic electricity for each dissolution process was 150 C, which corresponds to a dissolution depth of approximately 5 μm. Many hollows of several micrometers in diameter were present on the surface of the composite film deposited at an anodic current density of 1 A dm^{-2} (Fig. 2b). These hollows are formed by nonuniform dissolution of the Cu matrix, and may create defects such as voids in the Cu/MWCNT composite films during the PR electrodeposition process. Furthermore, the number of MWCNTs decreased compared to that prior to dissolution (Fig. 2a). The MWCNTs may be separated from the composite film surface during nonuniform dissolution of the Cu matrix. In contrast, there was a high density of MWCNTs in the composite film surface deposited at an anodic current density of 5 A dm^{-2} (Fig. 2c), and no hollows were observed. Thus, almost no MWCNTs separated from the composite film during the dissolution process at an anodic current density of 5 A dm^{-2}, in which the Cu matrix was uniformly dissolved. This could be caused by entanglement of the MWCNTs. At an anodic current density of 20 A dm^{-2}, no hollows were formed, and in contrast, the composite film had a very flat surface. However, there were few MWCNTs on the surface. It is considered that oxygen evolution may separate the MWCNTs from the composite film surface.

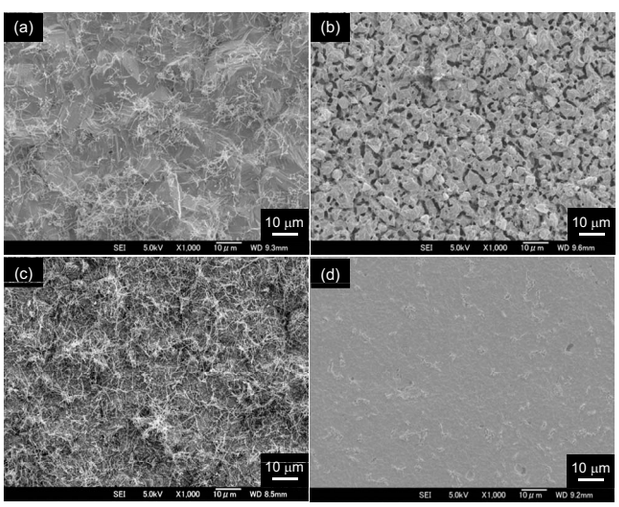

Figure 2. Surface FE-SEM images of Cu/MWCNT composite films after dissolution of the Cu matrix at various current densities: (a) before dissolution, and at (b) 1, (c) 5, and (d) 20 A dm^{-2}. The quantity of anodic electricity used was 150 C. The Cu/MWCNT composite film before the dissolution (a) was fabricated at 1 A dm^{-2} and its thickness was approximately 20 μm.

The nonuniform dissolution of the Cu matrix shown in Fig. 2b could be mainly attributed to electrochemical intergranular corrosion.[34] Dissolution of the Cu matrix may proceed mainly along the grain boundaries. In order to understand the nonuniform dissolution phenomena of the Cu matrix in detail, XRD measurements were conducted.

Figure 3 shows XRD patterns of the Cu/MWCNT composite films before and after the dissolution process. The thicknesses of the films were around 15 μm, so that there was little effect of the Cu substrate on the XRD patterns. All diffraction peaks were assigned to face-centered cubic Cu, and no peaks attributed to the MWCNTs were observed. The peak strength of the MWCNTs is considered to be very weak, thus, these patterns show only diffractions of the Cu matrix component of the Cu/MWCNT composite films before and after dissolution. The peak intensity ratios of the Cu crystal planes were somewhat different from each other. To clarify this difference, i.e., the difference in the orientation of the Cu films, the orientation index of each crystal plane was calculated.

Figure 4 shows the relationship between the anodic current density for the dissolution process and the orientation index for each crystal plane of the Cu matrix. The orientation index was calculated using Willson's equation[35]

Downloaded 02 Dec 2010 to 160.252.86.17. Redistribution subject to ECS license or copyright; see http://www.ecsdl.org/terms_use.jsp

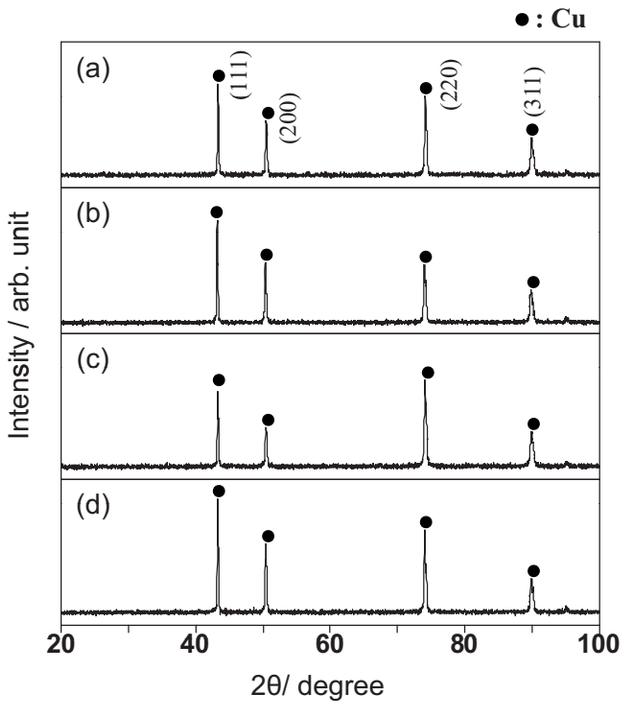

Figure 3. XRD patterns of the Cu/MWCNT composite films after dissolution at various anodic current densities: (a) before dissolution, and at (b) 1, (c) 5, and (d) 20 A dm^{-2}. The quantity of the anodic electricity used was 150 C. The Cu/MWCNT composite film before dissolution (a) was fabricated at 1 A dm^{-2} and its thickness was approximately 20 μm.

$$X(hkl) = \frac{\dfrac{I_m(hkl)}{\sum I_m(hkl)}}{\dfrac{I_{JCPDS}(hkl)}{\sum I_{JCPDS}(hkl)}}$$

where $X(hkl)$ is the orientation index of the observed crystal plane, $I_m(hkl)$ is the measured peak strength of the crystal plane, $\Sigma I_m(hkl)$ is the sum of the measured peak strengths for each crystal plane, $I_{JCPDS}(hkl)$ is the peak strength of the noted crystal plane in the JCPDS card, and $\Sigma I_{JCPDS}(hkl)$ is the sum of the peak strengths for each crystal plane in the JCPDS card. If $X(hkl)$ for the crystal plane is larger than 1, then the crystal plane is orientated perpendicularly against the film surface, and a higher orientation index value indicates stronger orientation of the crystal plane. In this study, (111), (200), (220), and (311) planes were taken into account. It is notable that the orientation index for the (220) plane is larger than 1 and has the highest value among these crystal planes. Furthermore, the orientation index for the (220) plane is clearly lower at 1 A dm^{-2} than at other current densities. The orientation indixes for other crystal planes did not change significantly at each current density. Therefore, it is thought that Cu crystallites with the (220) plane orientated perpendicularly against the film surface were selectively dissolved at an anodic current density of 1 A dm^{-2}. For the Cu face-centered cubic structure, the ascending order of surface free energy $\gamma_{(hkl)}$ is $\gamma_{(111)} < \gamma_{(100)} < \gamma_{(110)}$.[36] Therefore, the (220) plane is most unstable, i.e., the most soluble crystal plane among the (111), (200), and (220) planes. Beyond an anodic current density of 5 A dm^{-2}, the corresponding anode potentials of the film surfaces may be sufficiently high with respect to the differences of the surface free energy of each crystal plane. The difference of the dissolution rate between each crystal plane would become smaller, which would result in smooth surface morphologies at higher current densities.

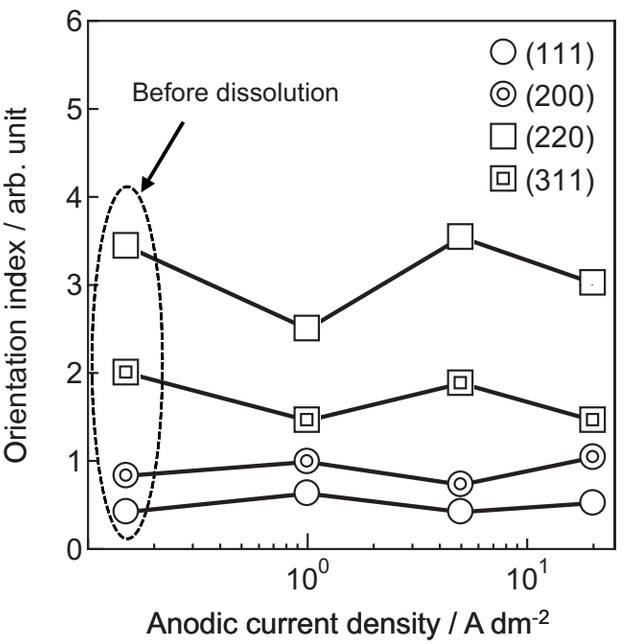

Figure 4. Relationship between anodic current density and the orientation index of Cu crystal planes. The (111), (200), (220), and (311) planes were taken into account.

Strictly speaking, the effect of the (311) plane should be considered, and this will be treated in future work. The dissolution current density affects the surface morphology of the composite film; therefore, the selection of an appropriate dissolution current density is important for the fabrication of compact composite films. From these results, the dissolution current density for the PR electrodeposition was set to 5 A dm^{-2}. The extra PA5000 dispersant that does not adsorb onto the MWCNTs may adsorb on the deposited copper surface and affect the behavior of PR electrodeposition. We plan to investigate the specific role of PA5000 during PR electrodeposition in future work.

Figure 5 shows the waveform used for PR electrodeposition in this study. The cathodic pulse current density was set to 1 A dm^{-2} (the cathodic pulse current i_c was 0.1 A and the surface area of the

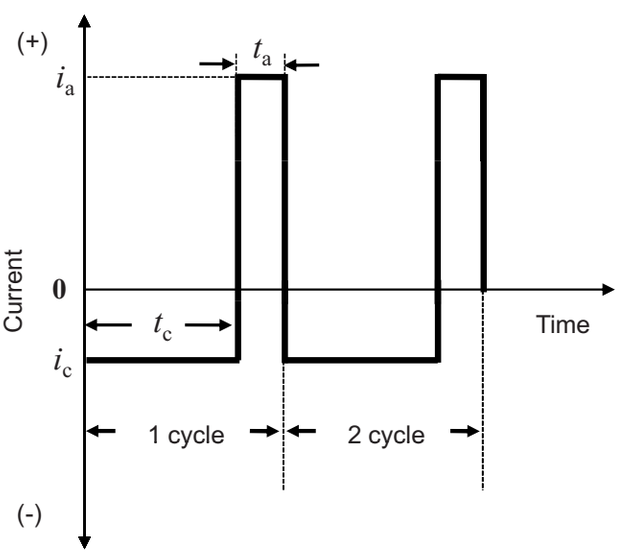

Figure 5. Waveform for PR electrodeposition.

Downloaded 02 Dec 2010 to 160.252.86.17. Redistribution subject to ECS license or copyright; see http://www.ecsdl.org/terms_use.jsp

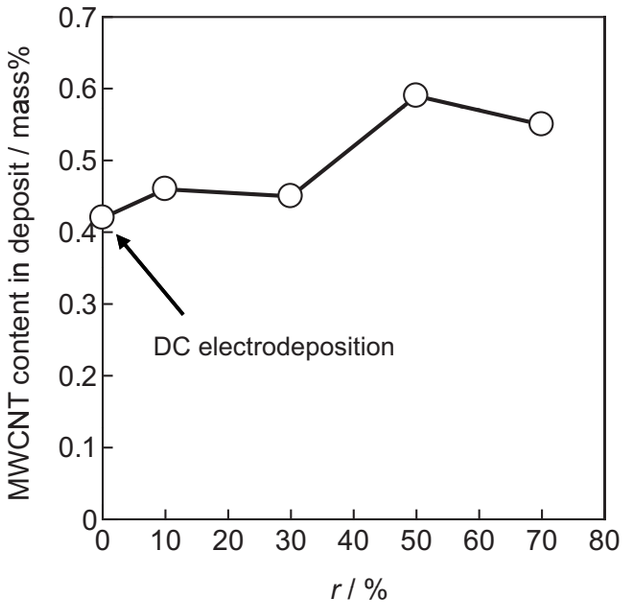

Figure 6. Relationship between r and MWCNT content in the composite films.

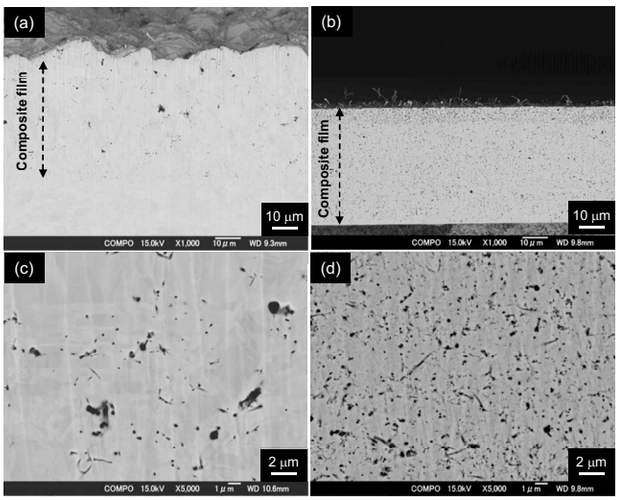

Figure 8. Cross-sectional FE-SEM images of Cu/MWCNT composite films fabricated by (a) dc and (b) PR electrodeposition (r = 50%). The images in (c) and (d) are high magnification images of (a) and (b), respectively.

substrate was 10 cm^2) and the cathodic pulse time t_c was 3000 s, which corresponds to a film thickness of around 10 μm. The anodic pulse current density was set to 5 A dm^{-2} (the anodic pulse current i_c was 0.5 A). The anodic pulse time t_a was varied and the reverse ratio r of the PR electrodeposition was defined as follows

$$r = \frac{i_a \times t_a}{i_c \times t_c} \times 100(\%)$$

The reverse rate r was varied from 0 to 70%.

Figure 6 shows the relationship between r and the MWCNT content in the composite films. The MWCNT content in the composite films increased with increasing r, and reached a maximum value of 0.59 mass % (r = 50%), which is an approximately 40% increase over that of the dc electrodeposited composite film (0.42 mass %). The MWCNT content decreased beyond r = 50%. At $r \geqslant 50\%$, more than 50% of the Cu matrix could be dissolved and the MWCNTs incorporated in the composite films would be easily separated, which would result in a decrease of the MWCNT content in the composite films.

Figure 7 shows a schematic illustration of the growth process for a Cu/MWCNT composite film by PR electrodeposition. First, the Cu/MWCNT composite film is grown on the substrate (Fig. 7a). The Cu matrix is selectively dissolved and almost all the MWCNTs contained in the dissolved Cu matrix remain on the film surface by entanglement, which results in a higher density of MWCNTs on the composite film surface, as shown in Fig. 2c (Fig. 7b). These processes occur during the first pulse cycle. During the second pulse cycle, more Cu/MWCNT composite is electrodeposited on the composite film surface that has a higher density of MWCNTs (Fig. 7c). These processes are repeated, which results in a higher MWCNT content of the composite film. Therefore, the results indicate that PR electrodeposition provides an increased MWCNT content in the composite films compared to that produced by dc electrodeposition.

Figure 8 shows cross-sectional FE-SEM images of Cu/MWCNT composite films fabricated using dc electrodeposition and PR electrodeposition. The quantities of net electricity for the fabrication of the films were both 1200 C, which corresponds to a film thickness of approximately 40 μm. The composite film produced using PR electrodeposition was fabricated by 8-cycle PR electrodeposition with r = 50%. The black areas in Fig. 8c and d are cross sections of the MWCNTs. A comparison of Fig. 8c and d confirms that the number of MWCNTs in the composite film fabricated by PR elec-

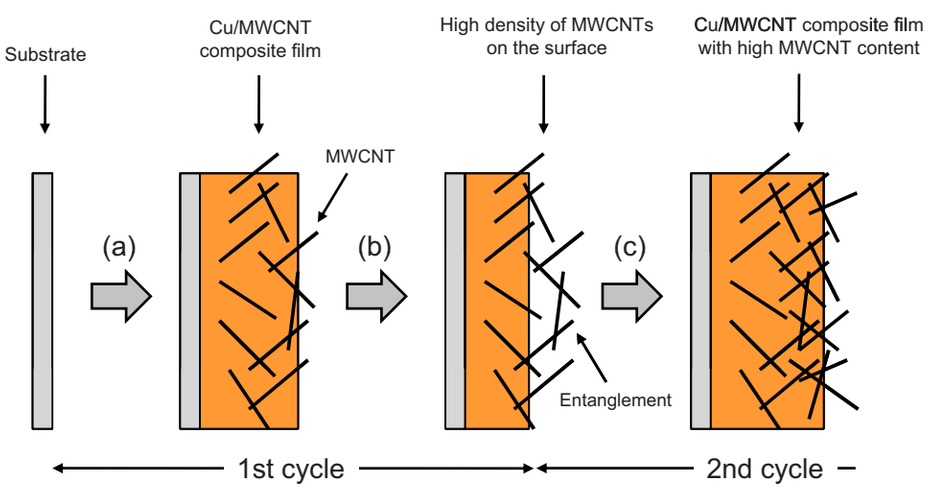

Figure 7. (Color online) Schematic illustration of the growth process for Cu/MWCNT composite films by PR electrodeposition. (a) Electrodeposition of Cu/MWCNT composite film on the substrate, (b) selective dissolution of Cu, and (c) electrodeposition of Cu/MWCNT composite film by a second pulse cycle.

Downloaded 02 Dec 2010 to 160.252.86.17. Redistribution subject to ECS license or copyright; see http://www.ecsdl.org/terms_use.jsp

trodeposition is higher than that fabricated by dc electrodeposition. There were no significant defects, such as voids in the Cu/MWCNT composite film produced by PR electrodeposition, as was the case for that produced by dc electrodeposition. This could be attributed to the choice of the anodic current density for the dissolution process. The surface roughness of the composite film fabricated by PR electrodeposition was smoother than that fabricated by dc electrodeposition (Fig. 8a and b). The PR electrodeposition process finishes with the dissolution process; therefore, a relatively smooth surface morphology was obtained.

Conclusions

PR electrodeposition was applied to increase the MWCNT content in Cu/MWCNT composite plating films. The electrodeposition and dissolution behavior of the composite films was investigated to determine suitable electrodeposition and dissolution current densities for PR electrodeposition. PR electrodeposition resulted in an increase of the MWCNT content in the composite films compared to composite films fabricated by dc electrodeposition. Furthermore, the surface roughness of the PR electrodeposited composite film was lowered compared to that prepared by dc electrodeposition.

Acknowledgments

This research was supported by Regional Innovation Cluster Program of Nagano, MEXT, Japan, and a Grant-in-Aid for Scientific Research (C) (grant no. 22560715) of JSPS, Japan.

Shinshu University assisted in meeting the publication costs of this article.

References

1. P. C. Andricacos, C. Uzoh, J. O. Dukovic, J. Horkans, and H. Deligianni, *IBM J. Res. Dev.*, **42**, 567 (1998).
2. J. J. Kelly and A. C. West, *Electrochem. Solid-State Lett.*, **2**, 561 (1999).
3. T. P. Moffat, J. E. Bonevich, W. H. Huber, A. Stanishevsky, D. R. Kelly, G. R. Stafford, and D. Josell, *J. Electrochem. Soc.*, **147**, 4524 (2000).
4. Y. Cao, P. Taephaisitphongse, R. Chalupa, and A. C. West, *J. Electrochem. Soc.*, **148**, C466 (2001).
5. D. Josell, D. Wheeler, W. H. Huber, and T. P. Moffat, *Phys. Rev. Lett.*, **87**, 016102 (2001).
6. M. Tan and J. N. Harb, *J. Electrochem. Soc.*, **150**, C420 (2003).
7. K. Kondo, T. Matsumoto, and K. Watanabe, *J. Electrochem. Soc.*, **151**, C250 (2004).
8. M. Hasegawa, Y. Negishi, T. Nakanishi, and T. Osaka, *J. Electrochem. Soc.*, **152**, C221 (2005).
9. W. P. Dow, H. S. Huang, M. Y. Yen, and H. C. Huang, *J. Electrochem. Soc.*, **152**, C425 (2005).
10. A. Tzanavaras, G. Young, and S. Gleixner, *J. Electrochem. Soc.*, **153**, C509 (2006).
11. J. Lee, J. Lee, J. Bae, W. Bang, K. Hong, M. H. Lee, S. G. Pyo, S. Kim, and J. G. Kim, *J. Electrochem. Soc.*, **153**, C521 (2006).
12. M. Tan, C. Guymon, D. R. Wheeler, and J. N. Harb, *J. Electrochem. Soc.*, **154**, D78 (2007).
13. C. C. Hung, W. H. Lee, S. C. Chang, K. W. Chen, and Y. L. Wang, *J. Electrochem. Soc.*, **155**, D133 (2008).
14. Y. B. Li, W. Wang, and Y. L. Li, *J. Electrochem. Soc.*, **156**, D119 (2009).
15. A. Oberlin, M. Endo, and T. Koyama, *J. Cryst. Growth*, **32**, 335 (1976).
16. S. Iijima, *Nature (London)*, **354**, 56 (1991).
17. X. H. Chen, J. C. Peng, X. Q. Li, F. M. Deng, J. X. Wang, and W. Z. Li, *J. Mater. Sci. Lett.*, **20**, 2057 (2001).
18. X. H. Chen, C. S. Chen, H. N. Xiao, X. B. Liu, L. P. Zhou, S. L. Li, and G. Zhang, *Tribol. Int.*, **39**, 22 (2006).
19. L. Shi, C. F. Sun, P. Gao, F. Zhou, and W. M. Liu, *Surf. Coat. Technol.*, **200**, 4870 (2006).
20. X. H. Chen, C. S. Chen, H. N. Xiao, F. Q. Cheng, G. Zhang, and G. J. Yi, *Surf. Coat. Technol.*, **191**, 351 (2005).
21. S. Arai, M. Endo, and N. Kaneko, *Carbon*, **42**, 641 (2004).
22. S. Arai, M. Endo, S. Hashizume, and Y. Shimojima, *Electrochem. Commun.*, **6**, 1029 (2004).
23. W. Feng, S. Arai, and M. Endo, *Electrochem. Commun.*, **6**, 1042 (2004).
24. S. Arai, M. Endo, T. Sato, and A. Koide, *Electrochem. Solid-State Lett.*, **9**, C131 (2006).
25. S. Arai, T. Saito, and M. Endo, *J. Electrochem. Soc.*, **154**, D530 (2007).
26. S. Arai and M. Endo, *Electrochem. Solid-State Lett.*, **7**, C25 (2004).
27. S. Arai and M. Endo, *Electrochem. Commun.*, **7**, 19 (2005).
28. S. Arai, T. Saito, and M. Endo, *J. Electrochem. Soc.*, **157**, D147 (2010).
29. S. Arai and M. Endo, *Electrochem. Commun.*, **5**, 797 (2003).
30. M. Endo, Y. A. Kim, T. Hayashi, K. Nishimura, T. Matsushita, K. Miyashita, and M. S. Dresselhaus, *Carbon*, **39**, 1287 (2001).
31. F. Wang, S. Arai, and M. Endo, *Electrochem. Commun.*, **7**, 674 (2005).
32. C. Guo, Y. Zuo, X. Zhao, J. Zhao, and J. Xiong, *Surf. Coat. Technol.*, **201**, 9491 (2007).
33. M. Endo, *CHEMTECH*, **18**, 568 (1988).
34. W. Luo, C. Qian, X. J. Wu, and M. Yan, *Mater. Sci. Eng., A*, **452–453**, 524 (2007).
35. K. S. Willson and J. A. Rogers, *Tech. Proc. Am. Electroplat. Soc.*, **51**, 593 (1964).
36. J. K. Mackenzie, A. J. W. Moore, and F. J. Nicholas, *J. Phys. Chem. Solids*, **23**, 185 (1962).

Downloaded 02 Dec 2010 to 160.252.86.17. Redistribution subject to ECS license or copyright; see http://www.ecsdl.org/terms_use.jsp